Progress In Electromagnetics Research C, Vol. 71, 111–122, 2017

Ultra-Compact Microstrip Antenna Array and Miniaturized Feeding Network

Wei Qiao[1], Xi Gao[1, 2, *], Xing Yang Yu[1], Si Min Li[1, 3], Yan Nan Jiang[1], and Hui Feng Ma[4]

Abstract—In this paper, an interdigital resonator that can greatly decrease mutual coupling between adjacent patches is proposed to realize an ultra-compact microstrip antenna array operating in 2.4 GHz wireless communication system. Due to its remarkable performance of decoupling, the edge to edge distance between adjacent patches can be reduced to $0.08\lambda_0$ and even less. Meanwhile, a miniaturized feeding network, which is composed of a CRLH-TL-based phase shifter and T-junction-based power divider, is used to feed the compact antenna array. The simulation results show that the proposed antenna array has an impedance bandwidth of 8.34%. We fabricate the antenna array to verify its performance. The experimental results are in good agreements with the simulations. Compared to the published designs, the proposed antenna array has an ultra-compact structure and hence can be used in space limited communication systems.

1. INTRODUCTION

Due to light weight, low profile, and easy processing, microstrip antenna arrays have been widely applied to many microwave and millimeter wave terminals, such as Multiple Input Multiple Output (MIMO) [1, 2], radar systems and air vehicles. On the other hand, with the rapid growth of modern wireless communication systems, these wireless terminals become more and more compact. When a microstrip antenna array is installed in such compact communication systems, we must reduce the size of the antenna array to adapt to the limited space. The reduction of antenna array will result in strong mutual coupling between radiation patches, which influences the system performance such as poor radiation patterns, input impedance mismatch, low signal-to-noise ratio and resonant frequency shift.

In order to solve the problem of mutual coupling, various advanced techniques, such as metamaterials [3], Frequency Selective Surface (FSS) [4], Single Negative material (SNG) [5], Electromagnetic Band Gap (EBG), and Defective Ground Structure (DGS), have been proposed. The EBG and DGS are favorable methods to suppress mutual coupling of antenna array due to their remarkable decoupling performance [6–8]. However, the EBG structure usually deteriorates the signal integrity. Although this problem can be solved by using un-planar compact EBG (UC-EBG), such a structure is more complicate, which makes it difficult to fabricate [9]. The DGS is formed by etching periodic slots on ground [10], in which the lattice constant of the periodic slots is so large that it cannot meet the demand of miniaturization. Furthermore, the slots etched on ground will increase the back radiation and then affect the radiation performance of antenna array. Recently, a tunable miniaturized

Received 6 November 2016, Accepted 24 January 2017, Scheduled 9 February 2017

* Corresponding author: Xi Gao (gao_xi76@163.com).

[1] School of Information and Communication, Guilin University of Electronic Technology, Guilin 541004, China. [2] Guangxi Key Laboratory of Wireless Wideband Communication & Signal Processing, Guilin, Guangxi 541004, China. [3] Guangxi University of Technology, Liuzhou 545006, China. [4] State Key Laboratory of Millimeter Waves, Department of Radio Engineering, Southeast University, Nanjing 210096, China.

decoupling antenna array has been proposed to realize high level isolation, but the antenna array has a complex structure [11]. Up to now, the reduction of mutual coupling is still a challenging, common and contradictive issue in communication systems. Especially for ultra-compact antenna array, the issue is more prominent. Therefore, some novel decoupling structures should be developed and studied to suppress the mutual coupling.

To match an ultra-compact antenna array, the size of the feeding network should be synchronously reduced. Usually, to feed electromagnetic (EM) wave with equal amplitude and phase to each element, the feeding network not only acts as power splitter but also has the role of phase shifter. For a conventional phase shifter, such as meander line, it is realized by phase accumulation, which makes the length of the device depend on operation wavelength. So this phase shifter occupies a large space and cannot be applied in an ultra-compact antenna array. In recent years, many phase shifters based on metamaterials including composite Right/Left Handed Transmission Lines (CRLH-TLs) are proposed to reduce their sizes [12, 13]. For example, a miniaturized Gysel power divider and phase shifter is realized by using CRLH-TLs implemented with lumped elements [14], in which a size reduction at least 81.8% is achieved. However, it is difficult to integrate the power splitter within the Microwave Monolithic Integrated Circuit (MMIC) due to the usage of lumped elements.

In this paper, we propose an ultra-compact antenna array consisting of a decoupling radiation array and a miniaturized feeding network based on CRLH-TLs. The decoupling array is formed by inserting two types of interdigital resonators between radiation patches. We show that these interdigital resonators can sharply decrease the mutual coupling between adjacent patches. By using these decoupling structures, the edge-to-edge distance of adjacent patches is decreased to $0.08\lambda_0$. At the same time, a miniaturized feeding network composed of CRLH-TLs and T-junctions is employed to feed EM energy to the antenna system. Both simulated and experimental results show that the antenna array has an impedance bandwidth of 8.34% with central frequency 2.4 GHz. The proposed ultra-compact antenna array can be used in compact communication systems.

This paper is organized as follows. Section 2 describes the working principle and basic design of the proposed decoupling structure. In Section 3, a miniaturized feeding network based on CRLH-TLs and T-junctions is designed to match the ultra-compact patch array. The investigation on the radiation performance of the decoupling array combined with the miniaturized feeding network is conducted in Section 4. Finally, conclusion is given in Section 5.

2. DESIGN AND CHARACTERISTIC OF DECOUPLING STRUCTURE

Figure 1(a) shows the physical model of a reference antenna array with three elements. In this patch array, the coupling between two adjacent elements are realized through all present media, i.e., substrate and air [15]. Furthermore, the coupled electromagnetic mode may be looked as a transverse electric and magnetic (TEM) wave whose wave vector is along the y axis and whose polarization direction of electric field is parallel to the x axis. Based on the characteristic of the coupled EM wave, the direct mutual coupling can be controlled by adding an extra decoupling structure. For a compact antenna array, the conventional decoupling structures such as split ring resonator (SRR), EBG and DGS can effectively suppress the mutual coupling. On the other hand, for an ultra-compact antenna array, for example the edge to edge distance less than $0.1\lambda_0$, these conventional decoupling structures may not be suitable for the realization of high isolation.

In order to realize high isolation for an ultra-compact patch array, an interdigital structure shown in Fig. 1(b) is employed. Fig. 1(c) illustrates the geometrical configuration of an antenna array, in which the proposed decoupling structure is inserted into the gap between patches. Here, the distance between two adjacent elements is only $0.08\lambda_0$; the operating frequency of the antenna element is 2.4 GHz; the bandwidth with $S_{11} \leq -10$ dB is 30 MHz (2.38 GHz $\sim$ 2.41 GHz). The patch array is fabricated on an FR4 substrate with relative dielectric constant of 4.4 and thickness of 0.8 mm.

With the help of electromagnetic field simulator Ansoft HFSS based on full-wave finite element method, we first study the decoupling characteristic of the proposed interdigital structure by simulating S parameter of the array shown in Fig. 1(c). In simulation, we only consider the isolation between F1 and F2 or F2 and F3, and do not consider the isolation between F1 and F3 because of their large distance (about $\lambda_0/2$). Fig. 2 illustrates the isolation between F1 and F2, i.e., S_{12} for different geometric

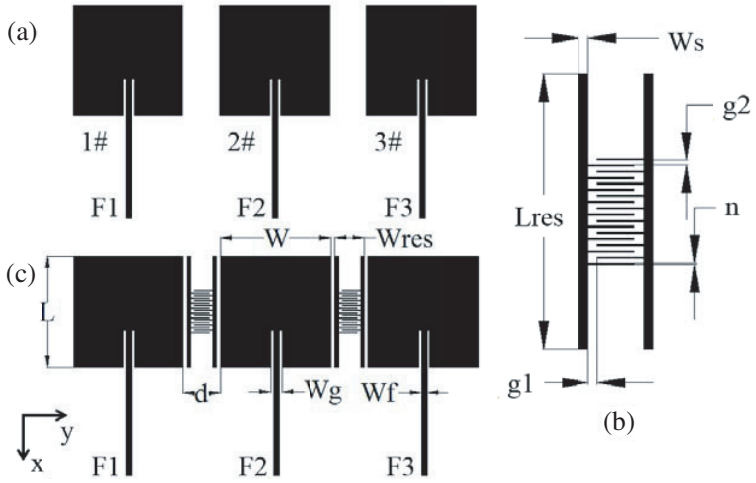

Figure 1. (a) The reference antenna array, (b) interdigital resonator for mutual coupling reduction and (c) the proposed antenna array, whose final geometrical parameters (in millimeter: mm) are $d = 10$, $L = 30$, $W = 30$, $L_{\text{res}} = 30$, $W_{\text{res}} = 8$, $W_g = 2.96$, $W_f = 1.53$, $W_s = 1$, $g1 = 1$, $g2 = 0.67$, $n = 0.17$.

parameters, such as $g2$, e, L_{res} and the number of fingers N. It is observed that these geometric parameters have great influence on S_{12} parameters. By changing the geometric parameters, we find that S_{12} exhibits a sharp dip at around 2.4 GHz. In the decoupling array, the interdigital resonator can be looked as a RLC resonant circuit, which is parallel to the radiation patches. Its resonant frequency is $\omega_0 = 1/\sqrt{L_d C_d}$, where L_d and C_d are equivalent inductance and equivalent capacitance, respectively. The increment of parameters $g2$, n and N will increase the equivalent capacitance (C_d). Similarly, the equivalent inductance (L_d) increases with the increment of L_{res}. Therefore, the resonant frequency ω_0 shifts to low frequencies when the above parameters are increased, as shown in Fig. 2. When the optimal parameters (see the caption of Fig. 1) are chosen, S_{12} reaches -60 dB. It implies the excellent decoupling performance of the proposed array.

In order to gain insight into the physical mechanism of the decoupling characteristic, we analyze the surface current distribution on the proposed decoupling array and compare it with reference antenna array (without decoupling structures). In simulation, F2 is set as excitation port, and the other ports (F1 and F3) are terminated with standard impedance matching loads. The simulated results are shown in Fig. 3. For the reference antenna array, the mutual coupling occurs through the dielectric substrate and the air over the patches, so strong induced currents appear on 1# and 3# patches, as shown in Fig. 3(a). On the other hand, for the proposed antenna array, the interdigital resonator should be further looked as a resonant filter. At operation frequency, it prevents the EM wave propagating from 2# patches to the adjacent patches (1# and 3# patches). From the surface current distribution shown in Fig. 3(b), it is clearly observed that the strong induced currents are trapped by the interdigital resonator and significantly reduce the induced currents on the 1# and 3# patches, demonstrating its filter characteristic. Due to the filter characteristic of the proposed interdigital resonator, the antenna array shows high level isolation.

The proposed antenna array is also fabricated and measured by using a vector network analyzer (AV36580) to experimentally verify its performance. Figs. 4(a) and 4(b) give the comparison of experimental and simulated S parameters, and Fig. 4(c) shows a photo of the test system. It is observed that the measured results are in good agreement with the simulated ones except a slight frequency shift (about 20 MHz). The discrepancies are likely caused by tolerances in fabrication and measurement. At operating frequencies, the simulated and measured S_{12} parameters are -15 dB and -19 dB for the reference array and are -60 dB and -40 dB for the proposed decoupling array. The S_{12} parameters of the decoupling antenna are obviously less than that of the reference array, demonstrating the perfect performance of the decoupling structure. Fig. 5 illustrates the comparison of simulated far-field radiation patterns between the proposed array and the reference antenna. It is observed that the

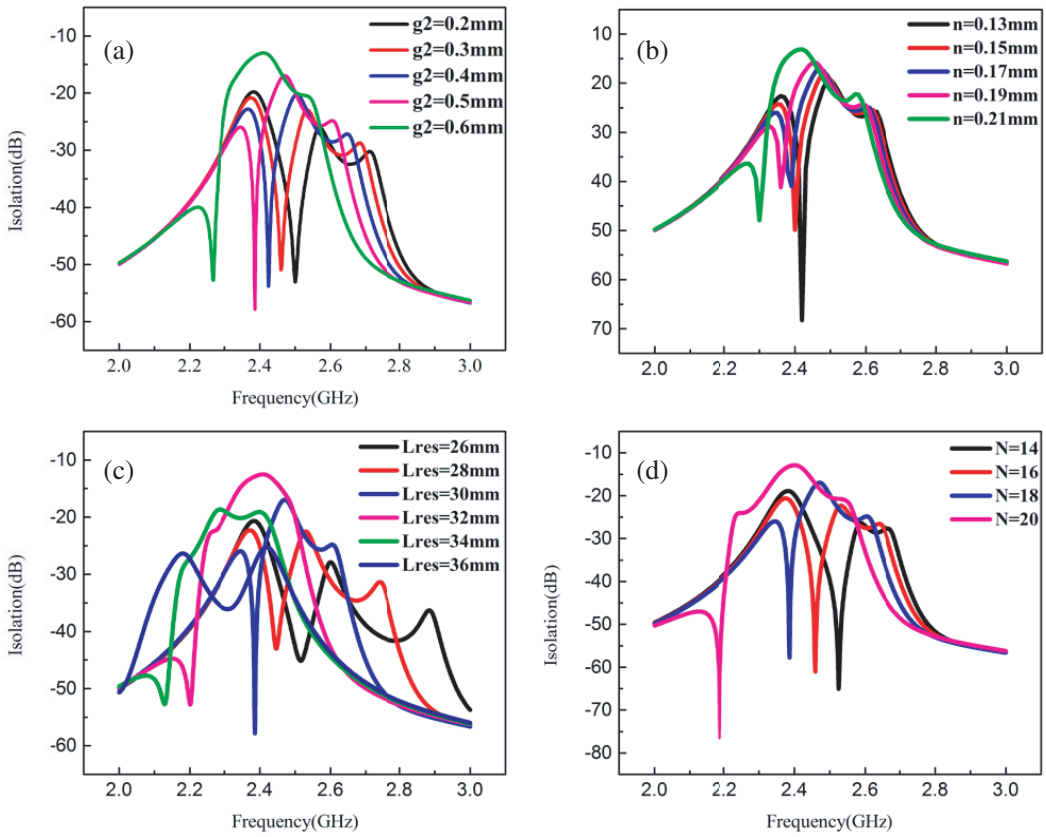

Figure 2. Isolation between the output ports (F1 and F2) against frequency with varied (a) $g2$, (b) n, (c) L_{res}, and (d) the number of fingers N.

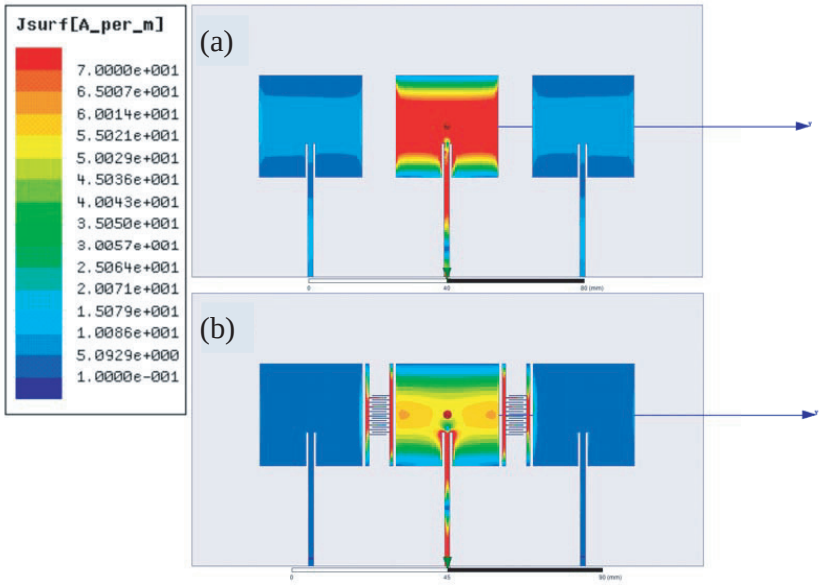

Figure 3. The surface current distributions on the top metallic plate of the antenna arrays at 2.4 GHz. (a) The reference antenna array, (b) the antenna array loaded with interdigital resonator.

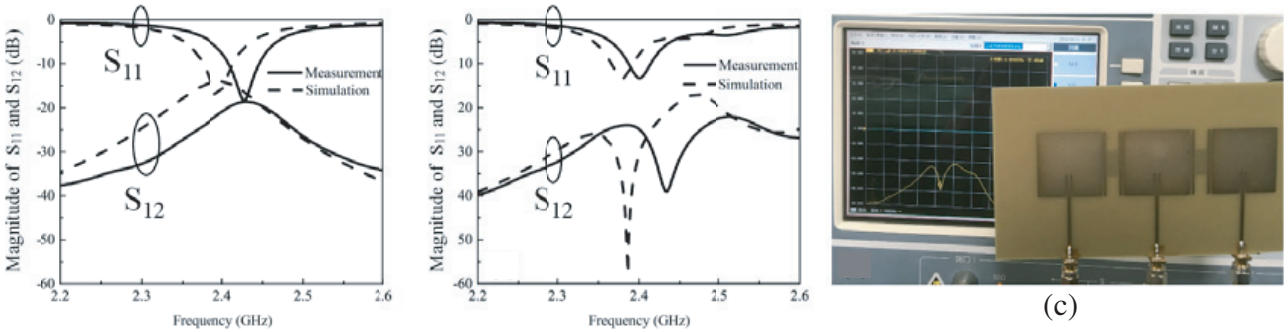

Figure 4. The measurement and simulated reflection coefficients (S_{11}) and mutual coupling coefficients (S_{21}) for the antenna arrays with and without interdigital resonator. (a) The reference antenna array, (b) the proposed antenna array, (c) the photo of the test system.

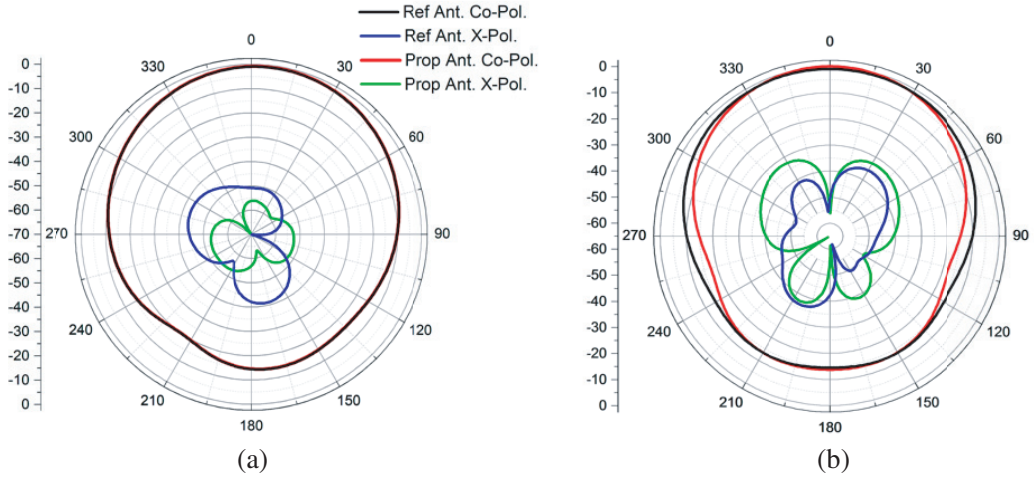

Figure 5. Radiation pattern of reference and proposed antenna array. (a) E plane, (b) H plane.

cross polarization of the proposed antenna is decreased, but the coplanar polarization is not changed, implying good performance of the proposed decoupling array.

The mutual coupling of the proposed array can also be quantitatively evaluated by using the Envelope correlation Coefficient (ECC). According to [16], the smaller the value of the ECC is, the higher isolation between adjacent elements is obtained. The ECC can be obtained from the following equation:

$$\rho_{ECC} = \frac{\left|S_{11} * S_{21} + S_{21} * S_{22}\right|^2}{\left(1 - \left|S_{11}\right|^2 - \left|S_{21}\right|^2\right)\left(1 - \left|S_{22}\right|^2 - \left|S_{12}\right|^2\right)} \tag{1}$$

where S_{11}, S_{12}, S_{22}, and S_{21} are S parameters between F1 and F2. Based on those simulated S parameters shown in Figs. 4(a) and 4(b), the ECCs are calculated, as shown in Fig. 6. It is observed that the maximal ECC of the proposed decoupling array is about 0.4, which is much smaller than that of the reference array. It again demonstrates the excellent decoupling characteristic of the proposed decoupling array.

Table 1 presents a comparison between the proposed decoupling array and other reported compact antenna arrays. From this table, one can see that the proposed decoupling structure has the strongest mutual coupling suppression and the shortest edge-to-edge distance (less than $0.1\lambda_0$). It is worth noting that the edge-to-edge distance can be further reduced by adjust the geometric parameters of

Table 1. Comparison between the proposed technique and other relevant methods.

Ref.	Technique	Centre frequency (in GHz)	Edge-to-edge spacing (λ_0)	Improvement in S_{21} (dB)
[3]	Waveguided metamaterials	3.5	0.125	6
[5]	SNG metamaterial	3.5	0.124	11.2
[9]	UC-EBG	5.75	0.5	10
[10]	DGS	6	0.5	18.28
[11]	Lumped resonator	2.44	0.12	20
[17]	Dual-band coupled resonator	2.4 and 5.2	0.077 and 0.17	10
Prop.	Interdigital resonator	2.4	0.08	21

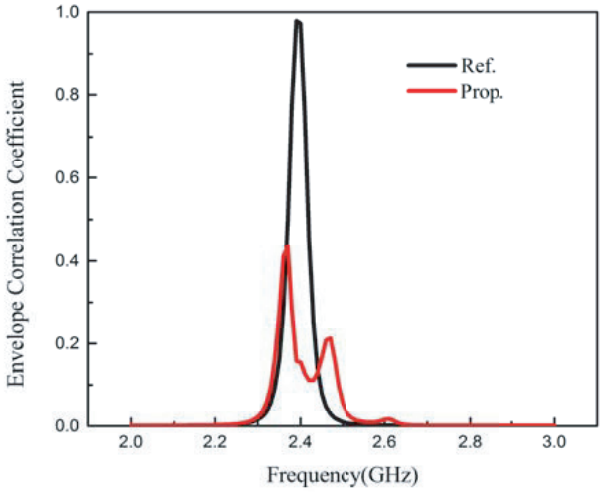

Figure 6. Envelope Correlation Coefficient of the antenna elements.

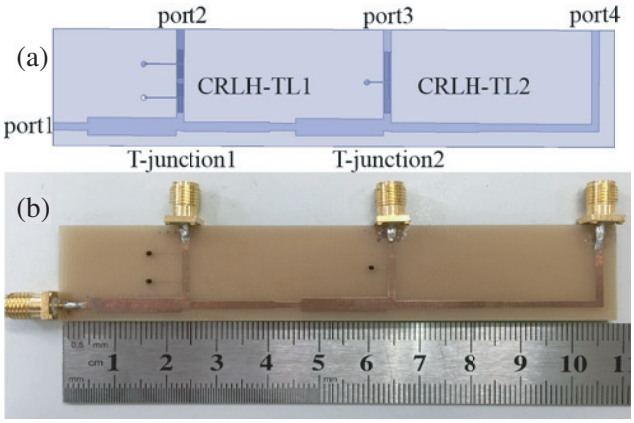

Figure 7. (a) The simulation model and (b) fabrication of the proposed feeding network.

the interdigital resonator. Further simulations show that the proposed decoupling structure still shows high isolation ($S_{12} = -54$ dB) when the edge-to-edge distance is decreased to 6 mm (about $0.048\lambda_0$). Considering the easiness of fabrication, we choose 10 mm as the edge-to-edge distance.

3. MINIATURIZED FEEDING NETWORK

To realize the miniaturization of feed network, we design a phase shifter by using three CRLH-TLs [18]. Fig. 7(a) shows the schematic configuration and fabrication of the feed network. Here, port 1 is used as input port and ports 2–4 set as output ports. Output ports 2–4 are respectively connected to ports F1–F3 shown in Fig. 1(c). Moreover, there are two phase shifters between port 2 and T-junction 1, and there is one phase shifter between port 3 and T-junction 2. These phase shifters are used to compensate the phase difference caused by the transmission line between port 2 and port 3 and between port 3 and port 4. By combining with these CRLH-TL-based phase shifters, the size of the feeding network is reduced greatly. The total length of the feeding network is only 105 mm (see Fig. 7(b)).

Figure 8(a) gives the fine structure of the phase shifter which is composed of two series interdigital capacitors and a stub inductor with terminal short circuit. The interdigital capacitor is treated as a quasi-lumped capacitor, and the shunt stub is looked as a shunt distributed inductance. Therefore, its equivalent circuit can be denoted as that shown in Fig. 8(b). According to [19], an arbitrary insertion phase shifting can be achieved by changing the parameters of interdigital capacitors, such as e, s, l_{cap},

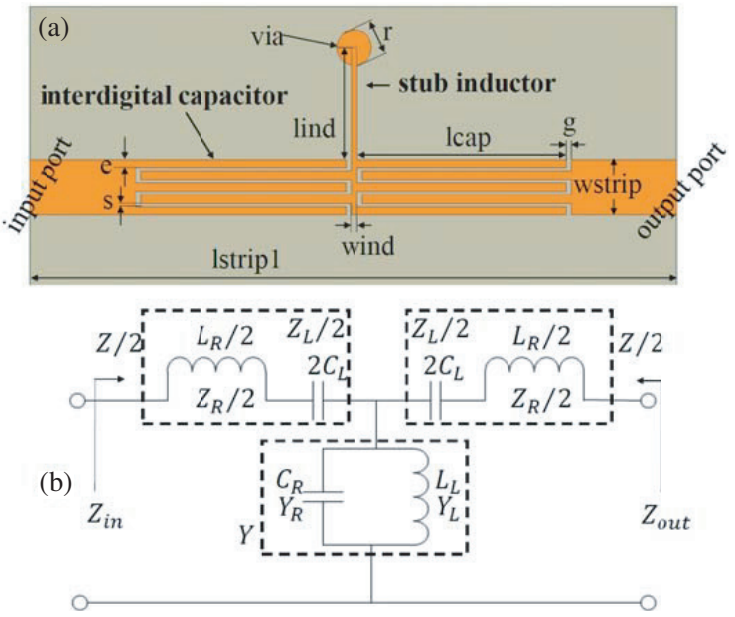

Figure 8. (a) Model of the CRLH-TL loaded microstrip line and (b) the equivalent circuit model of a symmetric CRLH-TL unit cell. Conventional transmission lines are modeled with series inductance (L_R) and shunt capacitance (C_R), while CRLH TL are modeled with L_R, C_R and series capacitance (C_L), shunt inductance (L_L).

g, and w_{strip}. Fortunately, the changes of these parameters do not significantly increase the size of phase shifter, and then a compact phase shifter is obtained.

For the equivalent circuit shown in Fig. 8(b), the phase difference (that is phase shift) between the output and input ports can be denoted as in the following equation [20, 21]:

$$\Delta\varphi \approx -\omega\sqrt{L_R C_R} + \frac{1}{\omega\sqrt{L_L C_L}} \tag{2}$$

where C_L is equivalent capacitance of the interdigital capacitors, and L_L is the equivalent inductance of the stub inductor. Parameters C_R and L_R are parasitic capacitance and inductance which are usually ignored due to their very small value. When we give a specific phase shift ($\Delta\varphi$), C_L and L_L can be calculated from Equation (2). Here, we suppose $\Delta\varphi = 4\pi/3$, then the obtained C_L and L_L are 2 pF and 1.24 nH, respectively.

On the other hand, capacitance C_L and inductance L_L also satisfy the following Equations (3) and (4) [22]:

$$C_{\text{interdigital}} = \left(\frac{\varepsilon_r + 1}{w_{\text{strip}}}\right) l_{\text{cap}} \left[\text{A}\left(\text{N} - 3\right) + \text{B}\right] \tag{3}$$

$$L_{\text{stub}} = A_1 l_{\text{ind}} \tag{4}$$

where N is the finger number of the interdigital; ε_r is the relative dielectric constant of the dielectric-slab; A and B are coefficients depending on the thickness of the substrate and the parameters of the fingers in interdigital resonator [22]; A_1 is the inductance per unit length of the stub inductor shown in Fig. 8(a). Here, we take $\varepsilon_r = 4.4$, $N = 5$, $A = 0.08$, $B = 0.09$, and $A_1 = 6.13\,\text{nH/ cm}$. $C_{\text{interdigital}}$ and L_{stub} are obtained from Equation (2), that is $C_{\text{interdigital}} = 2C_L = 4\,\text{pF}$ and $L_{\text{stub}} = L_L/2 = 2.48\,\text{nH}$. By substituting these parameters into Equations (3) and (4), we can get the initial values of the parameters l_{cap}, w_{strip} *and* l_{ind}, which are 11.39 mm, 1.53 mm, and 3.1 mm, respectively. Then, with the help of HFSS, the optimal parameters are obtained by optimizing these initial values.

Under these obtained optimal parameters, Fig. 9 presents S parameters of the proposed phase shifter (CRLH-TL1). For the convenience of comparison, S parameters of conventional microstrip line

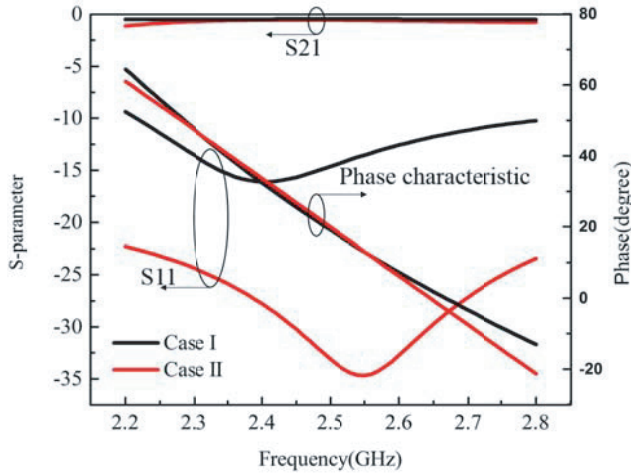

Figure 9. Comparison of S-parameter and phase characteristic for conventional microstrip line (Case II) and microstrip line loaded with CRLH-TL unit (Case I). Width of the both transmission line is $w_{\text{strip}} = 1.53$ mmlengths of Case I and Case II are $l_{\text{strip1}} = 18$ mm and $l_{\text{strip2}} = 60$ mm respectively.

are also given. From Fig. 9, we see that, in the frequency range from 2.2 GHz to 2.7 GHz, the phase of S parameter in the proposed phase shifter is approximately equal to that in conventional microstrip line. However, the length of the proposed shifter is only 18 mm which is much shorter than the length of microstrip line (60 mm), implying the realization of compact phase shifter. For CRLH-TL2, we can also get its optimal parameters by using the same method as CRLH-TL1. Table 2 exhibits the last parameters of the proposed phase shifters.

Table 2. Parameters of the phase shifters.

Parameter	Value (mm)	Parameter	Value (mm)
l_{cap_1}	5.23	l_{cap_2}	11.39
w_{ind_1}	0.17	w_{ind_2}	0.21
g_1	0.13	g_2	0.4
e_1	0.23	e_2	0.22
s_1	0.08225	s_2	0.09475
l_{ind_1}	6.2	l_{ind_2}	3.1
r	0.5	w_{strip}	1.53

For the T-junctions shown in Fig. 8(a), we take T-junction 1 as an example to analyze its characteristic by using circuit method. Fig. 10 shows the circuit of the T-junction 1, in which Z_1, Z_2, Z_3, Z_4 and Z_5 are the actual impedances of the transmission lines along the arrow directions, and Z_{02}, Z_{03}, and Z_{05} are the characteristic impedances of the transmission lines. P_1, P_2 and P_{in} represent the input or output powers of each port. Then the geometric parameters of the T-junction 1 can be achieved by using the method proposed in [23]. Table 3 illustrates the parameters of T-junction 1 and T-junction 2, based on which port 2, port 3 and port 4 can get equal output power when port 1 is excited.

To verify the performance of the proposed feeding network, we measure its S parameters and compare these results with simulations, as shown in Fig. 11. In experiment, the method is similar to the measurement of S parameters in Fig. 4(c). For example, to get S_{21}, port 1 and port 2 are input port and output port, respectively, while the other ports such as port 3 and port 4 are terminated with standard impedance matching loads. S_{31} and S_{41} are also tested by the same method. From Fig. 11, we

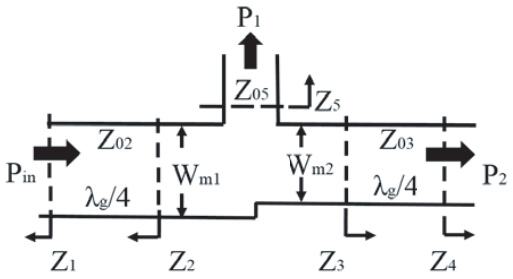

Figure 10. The schematic figure of the T-junction 1.

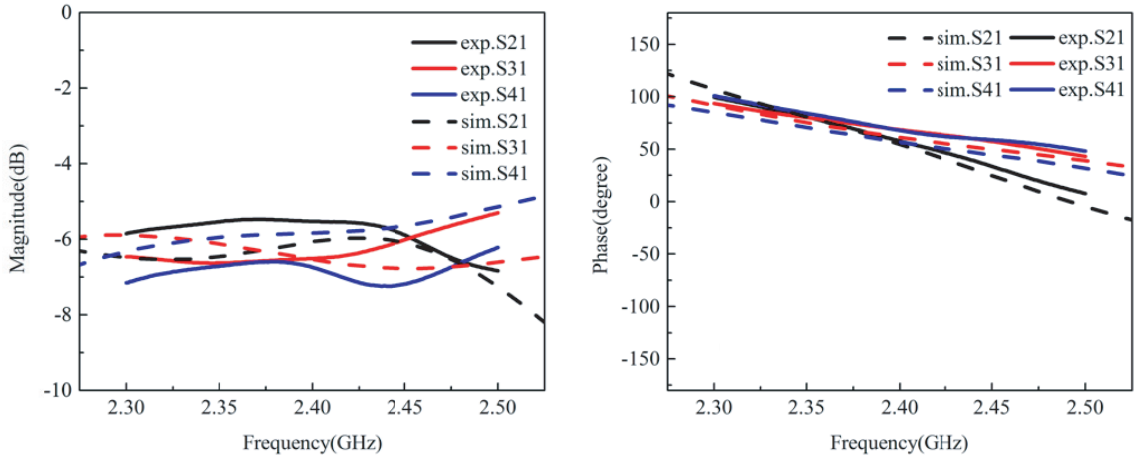

Figure 11. S parameters obtained by experiment and simulation method. (a) Magnitude of S parameters, (b) phase of S parameters.

Table 3. Parameters of the T-junctions.

Parameter	Value (mm)
W_{m1}	3.5
W_{m2}	1.9
W_{m3}	2.2
W_{m4}	1.8

see that the experimental results are in good agreement with the simulated ones. In the frequency range from 2.35 GHz to 2.42 GHz, the magnitudes of S_{21}, S_{31}, and S_{41} are approximately equal. Moreover, the phase difference of these S parameters is controlled within 10°. These results demonstrate good performance of the miniaturized network. However, the experimental magnitude of S_{21} is about 0.8 dB which is higher than that of S_{31} and S_{41}. It may be caused by the fabrication tolerances.

4. CO-SIMULATION AND EXPERIMENTAL RESULTS

According to the aforementioned results and guidelines, the whole structure of the compact antenna array is obtained as shown in Fig. 12(a). Fig. 12(b) presents a photo of the fabricated prototype. The comparison of the experimental and simulated results is presented in Fig. 13. From Fig. 13(a), we see

that the impedance bandwidth ($S_{11} \leq -10\,\text{dB}$) is 8.34% (2.35 GHz–2.55 GHz), which is slightly larger than the simulation result. This increment in experimental result may be caused by the loss of the dielectric plate. Fig. 13(b) displays the far-field patterns in E- and H-planes at the resonant frequency (2.4 GHz). In our test system, the rotating platform can only rotate from 90° to −90°, which makes the experimental results not show the back radiation. From Fig. 13(b), we also see that the measured half-power beamwidths (HPBWs) in H- and E-plane are 43.5° and 61.5°, respectively. However, the simulated HPBWs are 40° and 70°, respectively. From Fig. 11(a), we know that the experimental magnitude of S_{21} is about 0.8 dB which is higher than that of S_{31} and S_{41}. It may be the main cause of the discrepancy between experimental and simulated HPBWs. In addition, the simulated and measured gains of the proposed antenna array are 3.9 dB and 2.5 dB, respectively. In all, the experimental results show good agreement with simulations, demonstrating good performance of the proposed compact antenna array.

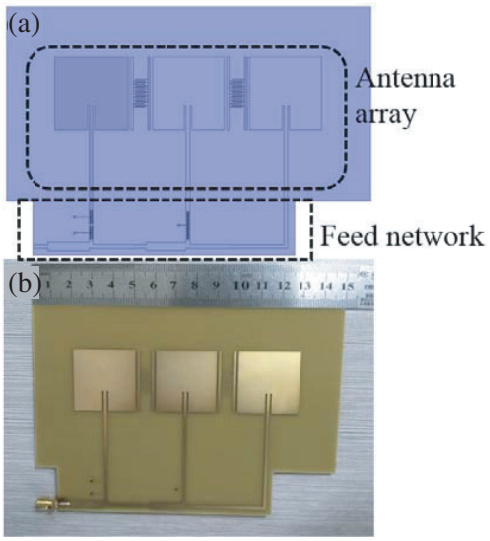

Figure 12. (a) The model of antenna array including miniaturized feeding network, (b) the photo of the fabricated antenna array.

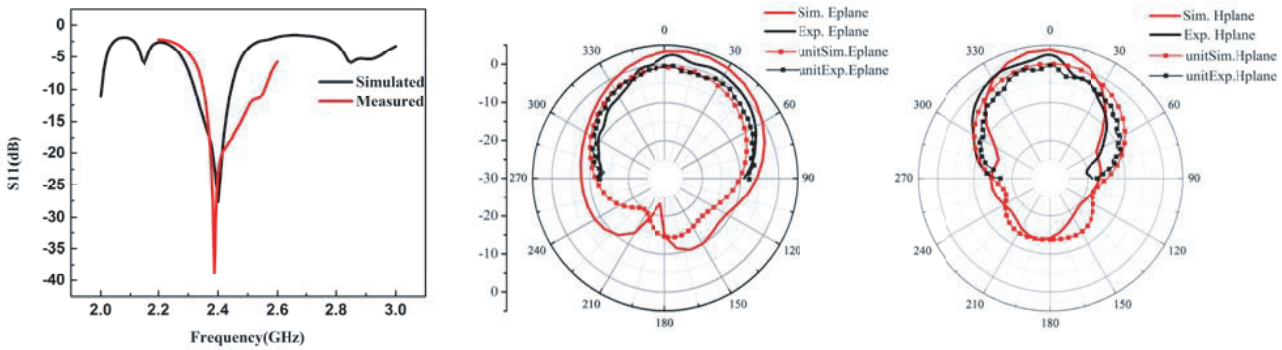

(a) (b)

Figure 13. (a) Simulated and measured S_{11} of the proposed antenna array with feeding network, (b) comparison of measured and simulated radiation patterns between the antenna array and the array element at 2.4 GHz.

5. CONCLUSION

In summary, we present an ultra-compact antenna array and its feeding network. By introducing interdigital resonator, the EM coupling between two adjacent patches is significantly reduced. Thanks to the decoupling characteristic, the edge-to-edge distance between two adjacent patches can be decreased to $0.08\lambda_0$ and even less, which results in the realization of ultra-compact antenna array. Moreover, a miniaturized network based on CRLH-TLs and T-junctions is employed to match the ultra-compact antenna array. To experimentally verify the performance of the proposed design, we fabricate a sample of the antenna array including feeding network. Both the simulation and measurement results show that the proposed antenna array has good radiation performance.

ACKNOWLEDGMENT

This work was supported in part by the National Natural Science Foundation of China under Grants 61461016, 61571117, and 61631007, in part by Natural Science Foundation of Guangxi under Grant 2014GXNSFAA118366 and 2015jjBB7002, and in part by the Innovation Project of GUET Graduate Education under Grant No. 2016YJCX82.

REFERENCES

1. Ouyang, J., F. Yang, and Z. M. Wang, "Reducing mutual coupling of closely spaced microstrip MIMO antennas for WLAN application," *IEEE Antennas and Wireless Propagation Letters*, Vol. 10, 310–313, 2011.
2. Sarkar, D., A. Singh, K. Saurav, and K. V. Srivastava, "Four-element quad-band multiple-input-multiple-output antenna employing split-ring resonator and inter-digital capacitor," *IET Microwaves, Antennas and Propagation*, Vol. 9, No. 13, 1453–1460, 2015.
3. Yang, X. M., X. G. Liu, X. Y. Zhou, and T. J. Cui, "Reduction of mutual coupling between closely packed patch antennas using waveguided metamaterials," *IEEE Antennas and Wireless Propagation Letters*, Vol. 11, 389–391, 2012.
4. Bernety, H. M. and A. B. Yakovlev, "Reduction of mutual coupling between neighboring strip dipole antennas using confocal elliptical metasurface cloaks," *IEEE Transactions on Antennas and Propagation*, Vol. 63, No. 4, 1554–1563, 2015.
5. Xu, H. X., G. M. Wang, M. Q. Qi, and H. Y. Zeng, "Ultra-small single-negative electric metamaterials for electromagnetic coupling reduction of microstrip antenna array," *Optics Express*, Vol. 20, 21968–21976, Sep. 2012.
6. Al-Hasan, M. J., T. A. Denidni, and A. R. Sebak, "Millimeter-wave compact EBG structure for mutual coupling reduction applications," *IEEE Transactions on Antennas and Propagation*, Vol. 63, No. 2, 823–828, 2015.
7. Yang, F. and Y. Rahmat-Samii, "Microstrip antennas integrated with electromagnetic band-gap (EBG) structures: A low mutual coupling design for array applications," *IEEE Transactions on Antennas and Propagation*, Vol. 51, No. 10, 2936–2946, 2003.
8. Park, J. S., J. S. Yun, and D. Ahn, "A design of the novel coupled-line bandpass filter using defected ground structure with wide stopband performance," *IEEE Transactions on Microwave Theory and Techniques*, Vol. 50, No. 9, 2037–2043, 2002.
9. Farahani, H. S., M. Veysi, M. Kamyab, and A. Tadjalli, "Mutual coupling reduction in patch antenna arrays using a UC-EBG superstrate," *IEEE Antennas and Wireless Propagation Letters*, Vol. 9, 57–59, 2010.
10. Salehi, M. and A. Tavakoli, "A novel low mutual coupling microstrip antenna array design using defected ground structure," *International Journal of Electronics and Communications (AEU)*, Vol. 60, No. 10, 718–723, 2006.
11. Qian, K. and D. Gan, "Compact tunable network for closely spaced antennas with high isolation," *Microwave and Optical Technology Letters*, Vol. 58, No. 1, 65–69, 2016.

12. Vélez, P., J. Bonache, and F. Martín, "Dual and broadband power dividers at microwave frequencies based on composite right/left handed (CRLH) lattice networks," *Photonics and Nanostructures — Fundamentals and Applications*, Vol. 12, No. 4, 269–278, 2014.
13. Bemani, M. and S. Nikmehr, "Nonradiating arbitrary dual-band equal and unequal 1 : 4 series power divider based on CRLH-TL structures," *IEEE Transactions on Industrial Electronics*, Vol. 61, No. 3, 1223–1234, 2015.
14. Ren, X., K. Song, F. Zhang, and B. Hu, "Miniaturized gysel power divider based on composite right/left-handed transmission lines," *IEEE Microwave Theory and Wireless Component Letters*, Vol. 25, No. 1, 22–24, 2015.
15. Ghosh, J., S. Ghosh, D. Mitra, and S. R. B. Chaudhuri, "Mutual coupling reduction between closely placed microstrip patch antenna using meander line resonator," *Progress In Electromagnetics Research Letters*, Vol. 59, 115–122, 2016.
16. Blanch, J., J. Romeu, and I. Cordella, "Exact representation of antenna system diversity performance from input parameter description," *Electronics Letters*, Vol. 39, No. 9, 705–707, 2003.
17. Zhao, L. and K. Wu, "A dual-band coupled resonator decoupling network for two coupled antennas," *IEEE Transactions on Antennas and Propagation*, Vol. 63, No. 9, 2843–2850, 2015.
18. Lin, X. Q., D. Bao, H. F. Ma, and T. J. Cui, "Novel composite phase-shifting transmission-line and its application in the design of antenna array," *IEEE Transactions on Antenna and Propagation*, Vol. 58, No. 2, 375–380, 2010.
19. Caloz, C. and T. Itoh, "Transmission line approach of left-handed (LH) materials and microstrip implementation of an artificial LH transmission line," *IEEE Transactions on Antennas and Propagation*, Vol. 52, No. 5, 1159–1166, 2004
20. Ludwing, R. and G. Bogdanov, *RF Circuit Design: Theory and Applications Chinese Simplified Language Edition*, 2nd edition, Publishing House of Electronics Industry, Beijing, 2013.
21. Cui, W., R. Wang, H. Zhang, J. Li, T. Hu, and Y. Liu, *Electromagnetic Metamaterials and Applications*, 2nd Edition, National Defense Industry Press, Beijing, 2014.
22. Alley, G. D., "Interdigital capacitors and their application to lumped-element microwave integrated circuits," *IEEE Transactions on Microwave Theory and Techniques*, Vol. 18, No. 12, 1028–1033, 1970.
23. Qiao, W., X. Gao, X. Yu, Y. Jiang, X. Yu, and W. Cao, "Compact power divider based on composite right/left-handed transmission line," *The 11th International Symposium on Antennas, Propagation and EM Theory*, to be published.